Catalysis Today 149 (2010) 35–39

Contents lists available at ScienceDirect

Catalysis Today

journal homepage: www.elsevier.com/locate/cattod

The relation between morphology of (Co)MoS_2 phases and selective hydrodesulfurization for CoMo catalysts

Mingfeng Li, Huifeng Li, Feng Jiang, Yang Chu, Hong Nie *

Research Institute of Petroleum Processing, SINOPEC, P.O. Box 914, 100083 Beijing, China

ARTICLE INFO

Article history:
Available online 15 April 2009

Keywords:
Alumina
Silica
Morphology
(Co)MoS_2
Edge/corner ratio
Selective hydrodesulfurization

ABSTRACT

A series of CoMo catalysts were prepared by various methods with three different supports (Al_2O_3-1 of γ phase, Al_2O_3-2 containing γ and δ mixed phases, SiO_2). And the effect of morphology of (Co)MoS_2 phases on selective hydrodesulfurization was studied systematically. The TEM images showed, in general, the average slab length, the stacking number and the ratio of edge/corner of the sulfided catalysts increase remarkably in the order: $SiO_2 > Al_2O_3$-2 > Al_2O_3-1, with the extent of metal–support interaction decreasing in the order: $SiO_2 < Al_2O_3$-2 < Al_2O_3-1. And the hydrodesulfurization selectivity correlates linearly with the slab length (or the ratio of edge/corner) of (Co)MoS_2 phases, the longer average slab length, the higher ratio of edge/corner, and then the better hydrodesulfurization selectivity. Among all the catalysts, sulfided CoMo/SiO_2 of the longest average slab length and the highest edge/corner ratio exhibits the best hydrodesulfurization selectivity.

1. Introduction

Clean gasoline (S <10 ppm) production as an important subject of environmental catalysis has received considerable attention in recent years [1–11]. And it is well known that FCC gasoline contains high levels of sulfur (0.005–1.5 wt.%), depending on whether the FCC feed stocks have been prehydrodesulfurized or not, and also a great quantity of olefins (20–40 wt.%), which provides it with a fairly good octane number [1,2]. However, during the process of hydrodesulfurization (HDS) of FCC gasoline, hydrogenation (HYD) reactions of olefins take place simultaneously and inevitably cause octane loss to some extent. So it is imperative to develop highly selective HDS catalysts so as to eliminate a maximum of the sulfur impurities with a minimum olefin saturation. So far, many studies have focused on the effects of reactivity of olefins, catalyst preparation parameters (increasing Co/Mo ratios, doping alumina with alkaline elements, adding chelating agents, etc.), sulfidation temperature and reaction conditions (hydrogen pressure, temperature, coking pretreatment, etc.) on selective HDS in CoMo/Al_2O_3 catalysts. And it is well accepted that the nature of the support plays an important role in the morphology and dispersion of the active metal phases and catalytic activity of the catalysts [12–17], but to the best of our knowledge, the correlation of morphology of (Co)MoS_2 phases and selective HDS has never been reported comprehensively in public. Therefore, the aim of this work is to prepare a series of CoMo catalysts by various methods to obtain (Co)MoS_2 phases of different morphology, and study the effect of morphology of (Co)MoS_2 phases on selective HDS.

2. Experimental

2.1. Catalyst preparation

Three different kinds of commercial supports Al_2O_3-1 (CLDT-1, SINOPEC Changling catalyst company), Al_2O_3-2 (CLDT-2, SINOPEC Changling catalyst company) and SiO_2 (Cukong-silica, Qingdao Haiyang chemical Company) were obtained without further treatment. The XRD patterns shown in Fig. 1 indicate Al_2O_3-1 of pure γ phase and Al_2O_3-2 of δ and γ mixed phases and silica of amorphous SiO_2 phase. In all of the preparation of catalysts, the incipient wetness impregnation method was used, with cobalt nitrate and ammonium heptamolybdate as the precursor of Co and Mo, respectively. CoMo/Al_2O_3-1, CoMo/Al_2O_3-2 and CoMo/SiO_2 were prepared by co-impregnation method with an ammonia solution of the Co and Mo salts, respectively. CoMo-EDTA/SiO_2 was prepared by co-impregnation of the solution containing the Co, Mo, and EDTA salts (the molar ratio of EDTA/Co = 2.0). Co/Mo-S/Al_2O_3-1 and Co/Mo-S/Al_2O_3-2 were prepared by the sequential impregnation of Co and Mo. First, Mo was impregnated, followed by drying at 393 K for 4 h and sulfiding (the details see the catalyst presulfidation below) at 593 K for 3 h; second, Co was impregnated. And the final metal loadings of all the catalysts as determined by XRF are approximately 2.5 wt.% CoO and 8 wt.%

* Corresponding author. Tel.: +86 10 82368928; fax: +86 10 62311290.
E-mail address: niehong@ripp-sinopec.com (H. Nie).

0920-5861/$ – see front matter © 2009 Elsevier B.V. All rights reserved.
doi:10.1016/j.cattod.2009.03.017

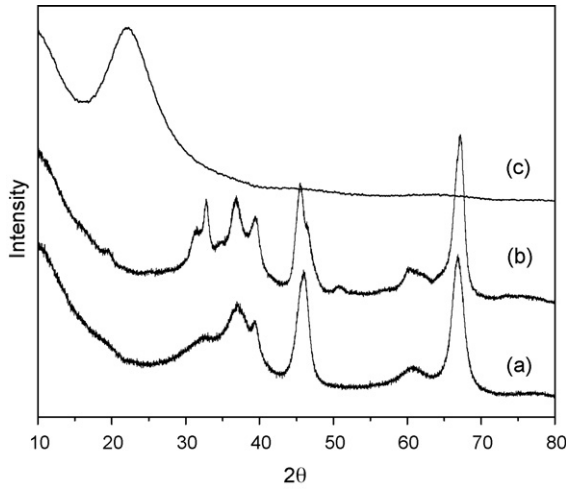

Fig. 1. X-ray diffraction patterns of (a) Al_2O_3-1, (b) Al_2O_3-2 and (c) SiO_2.

MoO_3. Prior to use, all the catalysts were dried at 393 K for 4 h, except Co/Mo-S/Al_2O_3-1 and Co/Mo-S/Al_2O_3-2 were dried under vacuum.

2.2. Characterization

X-ray diffraction (XRD) patterns were recorded on a Philips X'Pert diffractometer, using the Cu Kα radiation at 40 kV and 40 mA. The element contents of the catalysts were determined on a ZSX100e X-ray fluorescence analyzer. The transmission electron microscopy (TEM) images of the sulfided catalysts were recorded on a Tecnai G^2 F20 S-TWIN microscope. The catalysts were sulfided in a 15% H_2S/H_2 (by volume) flow of 100 cm^3/min, heating to 673 K at a rate of 6 K/min, then keeping at 673 K for 4 h. Subsequently, the sample was cooled to room temperature under flowing N_2. And the sample was milled in an agate mortar and ultrasonically suspended in cyclohexane. A drop of the supernatant liquid was placed on a copper grid coated with a sputtered carbon polymer. At least 10 representative micrographs were taken for each sample, and the average slab length ($\bar{L}$) and the stacking number ($\bar{N}$) were determined by manually measuring at least 150 slabs per sample. Considering that small sulfur-containing molecules (like thiophene) may not exhibit the rim/edge effect due to the absence of steric interference [18], the corner-edge model is used to describe the effect of morphology of (Co)MoS_2 phases on selective HDS. In accordance with the recent STM results of the promoted Co–Mo–S structures [19], it is found that Co promotion changes the morphology of the MoS_2 nanoclusters and that their shape becomes significantly more hexagonal. Therefore, these (Co)MoS_2 slabs are assumed as perfect hexagons. For these calculations, the published data of Kasztelan et al. [16] were employed. The number of Mo atoms along one side of a (Co)MoS_2 slab denoted as n'_i were determined from its length ($\bar{L} = 3.2 \times (2n'_i - 1)$) [16], that is, $n'_i = (10 \times \bar{L}/3.2 + 1)/2$. Besides, the number of Mo atoms at the edge sites (M_e), the number of Mo atoms at the corner sites (M_c) and the total number of Mo atoms (M_T) were calculated, respectively, by using the equations deduced by [15,16,20]. For the sake of clarity, all the formulae, related symbols and definitions for the morphology parameters of the (Co)MoS_2 slabs are listed in Table 1.

2.3. Catalytic activity evaluation

The catalytic activity tests were carried out in a continuous flow fixed-bed micro-reactor under the conditions: 1.6 MPa, 533 K, the catalyst loading of 1.00 g, 10 wt.% thiophene and 20 wt.% 1-hexene in heptane as the model feed, the feed flow rate of 0.16 cm^3/min, the H_2 flow rate of 360 cm^3/min. The catalysts were presulfided in situ with the sulfiding feed of 6 vol.% CS_2 in cyclohexane, 1.6 MPa and 593 K for 3 h. After steady-state conditions were reached, the liquid effluents were periodically auto-sampled and analyzed on-line by Agilent 6890N Gas Chromatograph with a 30 m capillary column OV-101. Finally, according to [21], the HDS activity, HYD activity and HDS selectivity factor of the catalysts were calculated as follows:

$$\text{HDS conversion } (X_T),\ \% = [(S_{feed} - S_{product})/S_{feed}] \times 100$$

where S_{feed} and $S_{product}$ denote the thiophene content in the feed and products, respectively.

$$\text{HYD conversion } (X_H),\ \% = [(H_{feed} - H_{product})/H_{feed}] \times 100$$

where H_{feed} and $H_{product}$ denote the hexene content in the feed and products, respectively.

$$\text{HDS selectivity factor } (S_T) = [\ln(1 - X_T)]/[\ln(1 - X_H)]$$

3. Results and discussion

3.1. Transmission electron microscopy

Representative TEM micrographs of six sulfided catalysts were shown in Figs. 2–4, exhibiting the well-known (Co)MoS_2 slab-like structure. The average slab length ($\bar{L}$), the stacking number ($\bar{N}$) and the ratio of f_e/f_c of the sulfided catalysts were summarized in Table 2. It is interesting to find that, in general, $\bar{L}$, $\bar{N}$ and f_e/f_c ratio of the sulfided catalysts remarkably increase in the order: SiO_2 > Al_2O_3-2 > Al_2O_3-1, with the extent of metal–support interaction decreasing in the order: SiO_2 < Al_2O_3-2 < Al_2O_3-1, as evidenced by the TPR results (the TPR profiles of the oxidic catalysts showed, the reduction

Table 1
Formulae for the morphology parameters of (Co)MoS_2 slabs.

Number	Formula	Symbol and definition
1	$\bar{L} = \frac{\sum l_i}{n}$	$\bar{L}$: the average slab length of (Co)MoS_2 slabs; n: the total number of slabs; l_i: the length of slab i.
2	$\bar{N} = \frac{\sum n_i N_i}{n}$	$\bar{N}$: the average stacking number of (Co)MoS_2 slabs; n_i: the number of stacks with N_i layers.
3	$n'_i = \frac{10^n \times \bar{L}/3.2 + 1}{2}$	n'_i: the number of Mo atoms along one side of a (Co)MoS_2 slab.
4	$Me = (6n'_i - 12)\bar{N}$	M_e: the number of Mo atoms at the edge sites.
5	$Mc = 6\bar{N}$	M_c: the number of Mo atoms at the corner sites.
6	$M_T = (3n'_i 2 - 3n'_i + 1)\bar{N}$	M_T: the total number of Mo atoms.
7	$f_e,\ \% = 100 \times M_e/M_T$	f_e: the fraction of Mo atoms at the edge sites.
8	$f_c,\ \% = 100 \times M_c/M_T$	f_c: the fraction of Mo atoms at the corner sites.
9	$f = f_e/f_c = n'_i - 2 = \frac{10 \times \bar{L}/3.2 - 3}{2}$	f: the ratio of f_e to f_c.

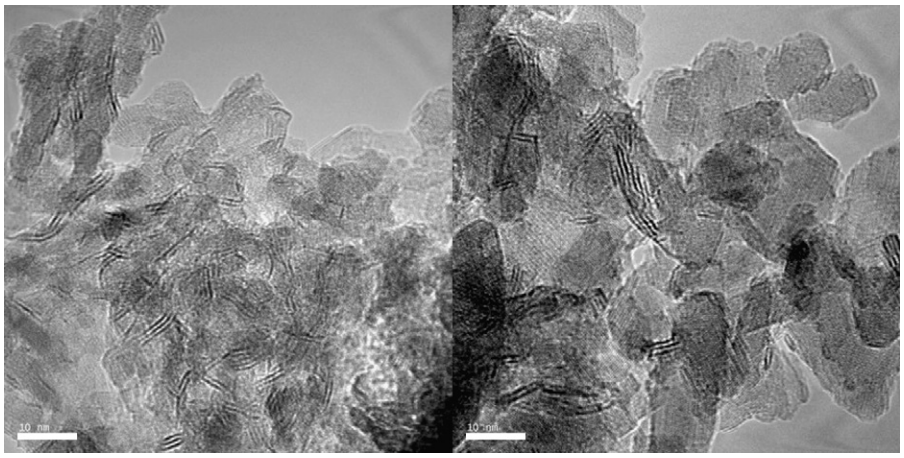

Fig. 2. TEM images of sulfided catalysts of $CoMo/Al_2O_3$-1 (left) and $CoMo/Al_2O_3$-2 (right).

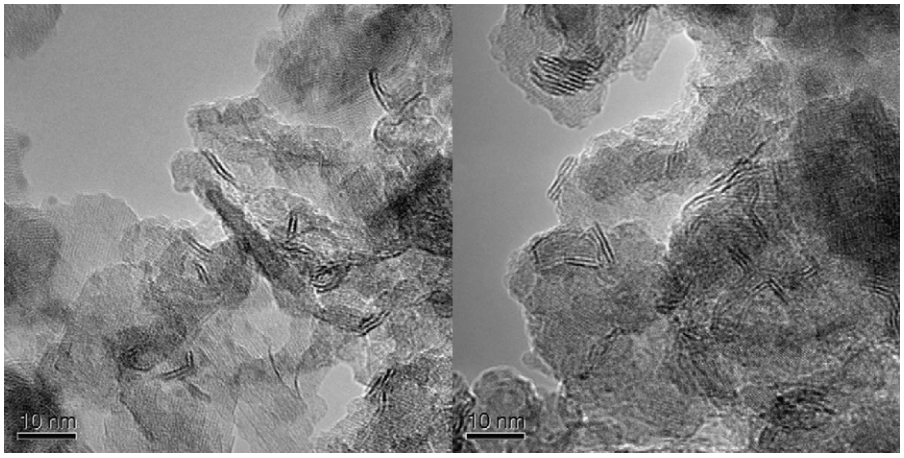

Fig. 3. TEM images of sulfided catalysts of $Co/Mo\text{-}S/Al_2O_3$-1 (left) and $Co/Mo\text{-}S/Al_2O_3$-2 (right).

peak of $CoMo/SiO_2$ shifts to lower temperature (1023 K) compared with those of $CoMo/Al_2O_3$-2 (1056 K) and $CoMo/Al_2O_3$-1 (1103 K), indicating that metal oxides are more easily reduced on SiO_2 than Al_2O_3-2 and Al_2O_3-1) [22]. To be specific, for Al_2O_3-1 supported catalysts, a higher f_e/f_c ratio for sulfided $Co/Mo\text{-}S/Al_2O_3$-1 than $CoMo/Al_2O_3$-1 was seen, ascribed to the increase in the average slab length of $(Co)MoS_2$ slabs after re-sulfidation. Similar results were also observed for $Co/Mo\text{-}S/Al_2O_3$-2 and $CoMo/Al_2O_3$-2. Compared with $CoMo/SiO_2$, the introduction of EDTA in the impregnation solution, decreases the average slab length of CoMo-EDTA/SiO_2 but slightly influences its average stacking number. It resulted in a lower f_e/f_c ratio for sulfided CoMo-EDTA/SiO_2 than $CoMo/SiO_2$.

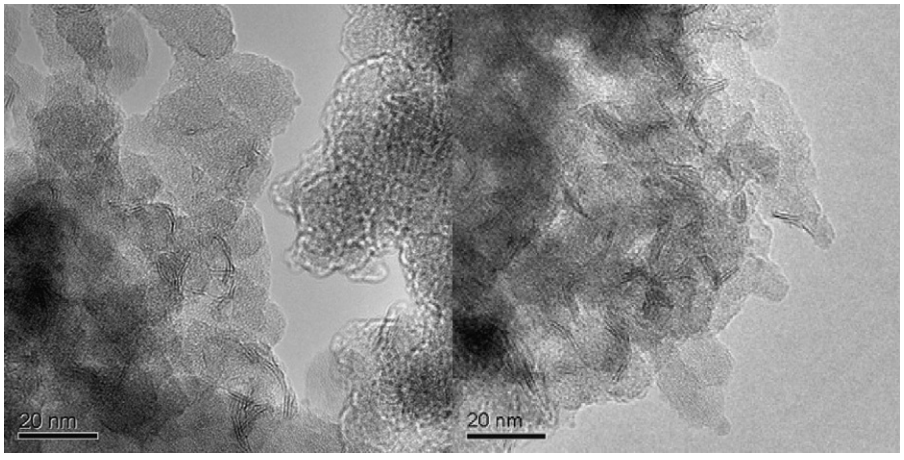

Fig. 4. TEM images of sulfided catalysts of $CoMo/SiO_2$ (left) and CoMo-EDTA/SiO_2 (right).

Table 2
The characteristics of the morphology of the sulfided catalysts.

Catalyst	Average slab length (nm)	Average stacking number	f_e	f_c	f_e/f_c
$CoMo/Al_2O_3$-1	4.8	2.2	21.3	3.6	5.9
$CoMo/Al_2O_3$-2	5.4	2.6	19.6	2.8	7.0
$Co/Mo-S/Al_2O_3$-1	5.3	2.1	19.7	2.9	6.8
$Co/Mo-S/Al_2O_3$-2	6.2	2.5	17.6	2.2	8.0
$CoMo/SiO_2$	6.6	2.7	16.9	1.9	8.9
$CoMo-EDTA/SiO_2$	6.3	2.7	17.8	2.2	8.1

3.2. Catalytic activity evaluation

The evaluation results of various catalysts were listed in Table 3. The HDS activity of the catalysts increase considerably in the order: $CoMo/Al_2O_3$-2 > $Co/Mo-S/Al_2O_3$-2 > $Co/Mo-S/Al_2O_3$-1 > $CoMo/Al_2O_3$-1 > $CoMo-EDTA/SiO_2$ > $CoMo/SiO_2$, but the HYD activity of the catalysts markedly increase in the order: $CoMo/Al_2O_3$-2 > $CoMo/Al_2O_3$-1 > $Co/Mo-S/Al_2O_3$-2 ≈ $Co/Mo-S/Al_2O_3$-1 > $CoMo-EDTA/SiO_2$ > $CoMo/SiO_2$. In general, the HDS and HYD activity of the catalysts approximately increase in the order: Al_2O_3-2 > Al_2O_3-1 > SiO_2. It can be explained that, on the one hand, apparently, the Al_2O_3-1 supported catalysts have more total active sites (edge sites and corner sites) than the corresponding Al_2O_3-2 supported catalysts as listed in Table 2, but stronger metal–support interaction for Al_2O_3-1 stimulates more Co to interact with Al_2O_3-1 instead of Mo than Al_2O_3-2, resulting in less formation of Co–Mo–S active phases and relative lower activity. On the other hand, compared with the Al_2O_3-1 and Al_2O_3-2 supported catalysts, the SiO_2 supported catalysts have fewer total active sites because of poorly dispersed (Co)MoS_2 phases with longer average slab length and higher stacking number due to its too weak metal–support interaction, just showing the lowest activity.

To be specific, for Al_2O_3-1 supported catalysts, the introduction of Co to the presulfided Mo/Al_2O_3-1 can apparently lead to a significantly higher decoration of the MoS_2 edges than conventional co-impregnation, because in the latter case the easier diffusion of Co ions into the alumina lattice to form cobalt spinel due to its strong metal–support interaction, in good agreement with the results of [23]. Moreover, because the promotion of Co on Mo increases markedly the C–S bond breaking reaction but in less extension influences the hydrogen transfer reactions as reported by [24], a higher HDS activity and lower HYD activity for sulfided $Co/Mo-S/Al_2O_3$-1 than $CoMo/Al_2O_3$-1 were seen.

For Al_2O_3-2 supported catalysts, contrary to the results of Al_2O_3-1 supported catalysts, a lower HDS activity and HYD activity for sulfided $Co/Mo-S/Al_2O_3$-2 than $CoMo/Al_2O_3$-2 were observed. It could be ascribed to that in the former case, its marked increase in the average slab length of (Co)MoS_2 slabs after re-sulfidation due to its moderate metal–support interaction, caused a decrease in total active sites than conventional co-impregnation, consisting well with the data listed in Table 2.

For SiO_2 supported catalysts, the introduction of EDTA in the impregnation solution, improves the dispersion of the metal precursors, decreases the average slab length of (Co)MoS_2 slabs and increases the total active sites, leading to a higher HDS activity and HYD activity for sulfided $CoMo-EDTA/SiO_2$.

In contrast, the HDS selectivity factors of the catalysts increase in the order: $CoMo/SiO_2$ > $CoMo-EDTA/SiO_2$ ≈ $Co/Mo-S/Al_2O_3$-2 > $Co/Mo-S/Al_2O_3$-1 ≈ $CoMo/Al_2O_3$-2 > $CoMo/Al_2O_3$-1. The reasons for the different performance of the catalysts will be explained below.

Table 3
Comparison of the HDS activity, HYD activity and HDS selectivity factor of various catalysts.

Catalyst	HDS (%)	HYD (%)	HDS selectivity factor
$CoMo/Al_2O_3$-1	33.6	54.8	0.5
$CoMo/Al_2O_3$-2	45.6	57.3	0.7
$Co/Mo-S/Al_2O_3$-1	36.1	46.3	0.7
$Co/Mo-S/Al_2O_3$-2	39.8	46.4	0.8
$CoMo/SiO_2$	10.2	9.8	1.0
$CoMo-EDTA/SiO_2$	23.8	28.3	0.8

3.3. The relation between morphology of (Co)MoS_2 phases and selective HDS

Considering that the shape of the (Co)MoS_2 phase is assumed as perfect hexagonal according to the STM results of the promoted Co–Mo–S structures [19], the edge/corner ratio is therefore a function of the slab length as listed in Table 1. To investigate the effect of morphology of (Co)MoS_2 phases on selective HDS, the correlation of HDS selectivity factor with the slab length of (Co)MoS_2 phases was illustrated in Fig. 5. It clearly exhibits that the HDS selectivity factor correlates linearly with the slab length of (Co)MoS_2 phases. Moreover, the longer average slab length indicates the higher ratio of edge/corner, and then the better HDS selectivity. And the reasons for this linear correlation can be explained as follows. On the one hand, there are two kinds of active sites on the (Co)MoS_2 slabs, edge sites and corner sites. According to the density functional theory computation results of [25], the corner sites are more favored thermodynamically for molecular hydrogen adsorption and dissociation into atomic hydrogen; moreover, the sulfur atoms associated with these corner Mo atoms are terminal ones, and sulfur removal from the corners is much easier than that from the edges. Thus, it results in a higher degree of coordinative unsaturation at the corner atoms than at the edge sites, and more favors HYD reaction at the corner sites, as reported by [15,16,26]. On the other hand, when the Mo atoms at edge sites are decorated by the Co atoms, the promoting effect of Co on Mo will essentially contributes to a noticeable increase in HDS activity but slightly influences HYD activity, as reported by [24]. Therefore, the higher edge/corner ratio of (Co)MoS_2 phases favors better HDS selectivity. And the sulfided $CoMo/SiO_2$ with the highest edge/corner ratio, just exhibits the best HDS selectivity.

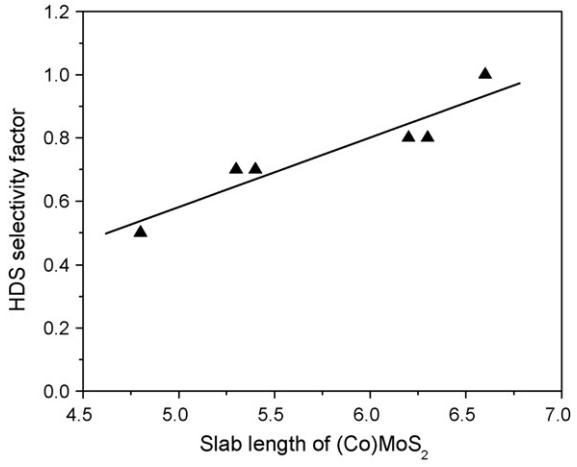

Fig. 5. The correlation of HDS selectivity factor with slab length of (Co)MoS_2.

4. Conclusion

A series of CoMo catalysts were prepared by various methods with three different supports (Al_2O_3-1 of γ phase, Al_2O_3-2 containing γ and δ mixed phases, SiO_2). The morphology of the sulfided catalysts was characterized by TEM, and the effect of morphology of (Co)MoS_2 phases on HDS selectivity was studied systematically. And the conclusions can be reasonably summarized as follows.

First, the TEM images showed, in general, the average slab length, the stacking number and the ratio of edge/corner of the sulfided catalysts increase remarkably in the order: $SiO_2 > Al_2O_3$-2 $> Al_2O_3$-1, with the extent of metal–support interaction decreasing in the order: $SiO_2 < Al_2O_3$-2 $< Al_2O_3$-1.

Second, HDS selectivity correlates linearly with the slab length of (Co)MoS_2 phases. It indicated that the longer average slab length, that is, the higher ratio of edge/corner, results in the better HDS selectivity. Among all the catalysts, sulfided CoMo/SiO_2 with the longest average slab length and the highest edge/corner ratio exhibits the best HDS selectivity.

Acknowledgments

The authors gratefully acknowledge the funding of the State Key Project (Grant 2006CB202506 and Grant 2007BAE43-B01).

References

[1] S. Bruneta, D. Meya, G. Pérota, C. Bouchyb, F. Diehl, Appl. Catal. A. 278 (2005) 143.
[2] T. Mochizuki, H. Itou, M. Toba, Y. Miki, Y. Yoshimura, Energ. Fuel. 22 (2008) 1456.
[3] G. Shi, H. Zhao, L. Song, J. Shen, Energ. Fuel. 22 (2008) 2450.
[4] M. Toba, Y. Miki, T. Matsui, M. Harada, Y. Yoshimura, Appl. Catal. B 70 (2007) 542.
[5] Y. Fan, J. Lu, G. Shi, H. Liu, X. Bao, Catal. Today 125 (2007) 220.
[6] M. Toba, Y. Miki, Y. Kanda, T. Matsui, M. Harada, Y. Yoshimura, Catal. Today 104 (2005) 64.
[7] J.T. Miller, W.J. Reagan, J.A. Kaduk, C.L. Marshall, A.J. Kropfy, J. Catal. 193 (2000) 123.
[8] M. Li, H. Nie, Y. Shi, D. Li, Stud. Surf. Catal. Sci. 127 (1999) 409.
[9] S. Hatanaka, M. Yamada, Ind. Eng. Chem. Res. 36 (1997) 1519.
[10] S. Hatanaka, M. Yamada, Ind. Eng. Chem. Res. 36 (1997) 5110.
[11] S. Hatanaka, M. Yamada, Ind. Eng. Chem. Res. 37 (1998) 1748.
[12] M. Breysse, P. Afanasiev, C. Geantet, M. Vrinat, Catal. Today 86 (2003) 5.
[13] Y. Okamoto, T. Kubota, Catal. Today 86 (2003) 31.
[14] H. Shimada, Catal. Today 86 (2003) 17.
[15] E.J.M. Hensen, P.J. Kooyman, Y. van der Meer, A.M. van der Kraan, V.H.J. de Beer, J.A.R. van Veen, R.A. van Santen, J. Catal. 199 (2001) 224.
[16] S. Kasztelan, H. Toulhoat, J. Grimblot, J.P. Bonnelle, Appl. Catal. 13 (1984) 127.
[17] E. Payen, R. Hubaut, S. Kasztelan, O. Poulet, J. Grimblot, J. Catal. 147 (1994) 123.
[18] M. Daage, R.R. Chianelli, J. Catal. 149 (1994) 414.
[19] F. Besenbacher, M. Brorson, B.S. Clausen, S. Helveg, B. Hinnemann, J. Kibsgaard, J.V. Lauritsen, P.G. Moses, J.K. Nørskov, H. Topsøe, Catal. Today 130 (2008) 86.
[20] D. Ferdous, A.K. Dalai, J. Adjaye, L. Kotlyar, Appl. Catal. A. 294 (2005) 80.
[21] R. Zhao, C. Yin, C. Liu, Am. Chem. Soc. Prepr. Div. Pet. Chem. 46 (2001) 30.
[22] M. Li, H. Li, F. Jiang, Y. Chu, H. Nie, unpublished results.
[23] H. TopsØe, B.S. Clausen, F.E. Massoth, in: J.R. Anderson, M. Boudart (Eds.), Catalysis: Science and Technology, vol. 11, Springer, Berlin, 1996, p. 76 (Chapter 3).
[24] S.L. González-Cortés, T.C. Xiao, P.M.F.J. Costa, B. Fontal, M.L.H. Green, Appl. Catal. A 270 (2004) 209.
[25] X. Wen, T. Zeng, B. Teng, F. Zhang, Y. Li, J. Wang, H. Jiao, J. Mol. Catal. A 249 (2006) 191.
[26] A. Wambeke, L. Jalowiecki, S. Kasztelan, J. Grimblot, J.P. Bonnelle, J. Catal. 109 (1988) 320.